



## Article

# The Influence of Surface Heterogeneity of Fluorite on the Adsorption of Alkyl Sulfonates

Yuhao He <sup>1</sup>, Zengzi Wang <sup>2</sup>, Zijie Ren <sup>1,3,\*</sup> , Renji Zheng <sup>4,5,\*</sup>, Huimin Gao <sup>1,3</sup> and Zhijie Chen <sup>6,\*</sup> 

<sup>1</sup> School of Resources and Environmental Engineering, Wuhan University of Technology, Wuhan 430070, China; he\_yuhao1998@163.com (Y.H.); gaohuimin1958@126.com (H.G.)

<sup>2</sup> CNBM Research Institute for Advanced Glass Materials Co., Ltd., Bengbu 233018, China; wangzengzi9622@163.com

<sup>3</sup> Hubei Key Laboratory of Mineral Resources Processing and Environment, Wuhan 430070, China

<sup>4</sup> Key Laboratory of Hunan Province for Clean and Efficient Utilization of Strategic Calcium-Containing Mineral Resources, Changsha 410083, China

<sup>5</sup> Key Laboratory of Hunan Province for Clean and Efficient Utilization of Strategic Calcium-Containing Mineral Resources, School of Minerals Processing and Bioengineering, Central South University, Changsha 410083, China

<sup>6</sup> Centre for Technology in Water and Wastewater, School of Civil and Environmental Engineering, University of Technology Sydney, Sydney, NSW 2007, Australia

\* Correspondence: renzijie@whut.edu.cn (Z.R.); zhengrj@csu.edu.cn (R.Z.); zhijie.chen@uts.edu.au (Z.C.)

**Abstract:** Surface heterogeneity of minerals can significantly affect the adsorption of collectors. Petroleum sulfonate is widely used as a fluorite collector, but how the surface heterogeneity of fluorite influences the adsorption of alkyl sulfonates remains unknown. Herein, two kinds of surface heterogeneity situations, i.e., edge and (1 1 1) \_vacancy, were modeled, and the adsorption of sodium dodecyl sulfonate on them was simulated. The results show that the stable adsorption configuration of sodium dodecyl sulfonate on the edge was in a bridged mode, and the stable interaction configuration with vacancy was in a tridentate mode. The 2p orbit of fluorine on the surface of the edge and the vacancy could hinder collector adsorption. After adsorption, the 3d orbit of calcium interacted with the collector orbit above Fermi level, and moved towards the lower energy level, benefiting the adsorption process. It was also found that the adsorption intensity/strength of alkyl sulfonate on fluorite was directly proportional to the interaction intensity of the collector with the 3d orbits of calcium ions on the surface and vacancy. Therefore, the rough fluorite surface had a stronger adsorption effect on the collector, and the existence of vacancy could improve the surface adsorption energy, and thus enhance the adsorption of the collector on the fluorite surface. The rough fluorite surface requires high collector concentration to achieve saturated monolayer adsorption, so increasing vacancy was the better choice to improve the adsorption capacity of alkyl sulfonate on the fluorite surface. This study provides novel insights into the flotation mechanism, in the context of surface heterogeneity, and could guide the design of high-performance collectors for fluorite ore flotation.

**Keywords:** fluorite; flotation; surface inhomogeneity; alkyl sulfonate; adsorption; collectors



**Citation:** He, Y.; Wang, Z.; Ren, Z.; Zheng, R.; Gao, H.; Chen, Z. The Influence of Surface Heterogeneity of Fluorite on the Adsorption of Alkyl Sulfonates. *Minerals* **2023**, *13*, 1005. <https://doi.org/10.3390/min13081005>

Academic Editor: Chiharu Tokoro

Received: 28 June 2023

Revised: 25 July 2023

Accepted: 26 July 2023

Published: 28 July 2023



**Copyright:** © 2023 by the authors. Licensee MDPI, Basel, Switzerland. This article is an open access article distributed under the terms and conditions of the Creative Commons Attribution (CC BY) license (<https://creativecommons.org/licenses/by/4.0/>).

## 1. Introduction

Fluorite is a critical raw material in different fields, such as metallurgy, building materials, new energy, and chemical industry [1]. The rapid economic development requires a growing demand for fluorite. Nevertheless, most natural fluorite ores cannot be used directly, and high-efficiency beneficiation is highly urgent. To date, the most widely used way to enrichment fluorite is froth flotation [2], and developing efficient flotation reagents (e.g., collectors) remains a central challenge. In flotation theories, the crystal structure and valence bond characteristics of minerals determine their natural floatability and the characteristics of reagent action [3]. For example, the non-uniformity of the fluorite surface will affect the adsorption of the collector on its surface [4]. The inhomogeneity

of the mineral surface includes physical inhomogeneity and chemical inhomogeneity. Physical inhomogeneity includes particle size inhomogeneity, surface inhomogeneity (edge, corners, unevenness, and pores), vacancy, and lattice defects, etc. Chemical inhomogeneity refers to the “solid solution” formed by isomorphism mixing into the mineral lattice [5]. The heterogeneity of the mineral surface not only affects the adsorption configuration, adsorption mechanism, and aggregation morphology of adsorbents, but also is one of the most important preconditions for the co-adsorption of various reagents.

As reported by Gao et al. [6], the common cleavage planes of fluorite are (1 1 1), (1 1 0), (1 0 0), and (3 1 0); of these, (1 1 1) is the main cleavage plane. Researchers have extensively studied the anisotropy of the fluorite crystal surface, and the surface anisotropy is reflected in the differences of surface energy, surface wettability, surface electricity, dissolution rate, surface adsorption, and other properties. The interaction strength between reagents and minerals affects the flotation performance, and studies on the anisotropy of the fluorite crystal plane also focus on the differences in the interactions between reagents and different crystal planes. Zheng et al. [7] have studied the difference in the adsorption characteristics of reagents on different crystal faces of fluorite. The activity of Ca atoms exposed on different surfaces was different, and the collector adsorption strength was also proportional to the activity of Ca atoms. Li and Gao [8] proposed that the flotation effect of fluorite can be improved by controlling the grinding method to produce more surfaces with highly active Ca atoms. Foucaud and coauthors [9] have studied the adsorption of oleic acid on the fluorite (1 1 1) surface. Among the three interaction modes (single coordination, double coordination, and bridge ring coordination), the double coordination was the most stable. The ideal dissociation of the fluorite (1 1 1) surface is along the two adjacent F-Ca-F layers, but the reality is that the dissociated surface is inhomogeneous (physical inhomogeneity). The fluorite (1 1 1) surface has been proven to have a step surface (1 1 1) [10,11], pyramid surface (kink) [12], and vacancy defect [13], etc. It could be inferred that these inhomogeneous areas also lead to different collector adsorption. Although some articles report the adsorption energy and adsorption configuration of the formic acid molecule [14] and the  $\text{CaF}_2$  molecule [15] on the fluorite surface and edge surfaces by using theoretical calculation methods, there are limited studies investigating the collectors' adsorption on the inhomogeneous area of fluorite.

Density functional theory (DFT) calculations can be utilized to study the interaction between the mineral surface and collector molecules, and the interaction mechanism of the collectors can be obtained by analyzing the electronic structure information, such as density of states [16], differential charge [17], and bond level [18]. Moreover, DFT calculations of the edge surface structure of the fluorite surface have shown that its atomic structure is similar to the (1 1 0) surface and (3 1 1) surface [12]. Therefore, studying the adsorption of collectors at the edge surface could determine their adsorption at (1 1 0) and (3 1 1).

Petroleum sulfonate is widely used in many industries, such as lubricating oil production, metal processing, petroleum production, the textile industry, and so on. Petroleum sulfonate has been used for the flotation of andalusite minerals, mica, quartz, silicate minerals, and ferromanganese minerals for a long time [19], and compared with sodium oleate [20], it has good low-temperature resistance [21]. However, the application of petroleum sulfonate in fluorite flotation is rarely studied, and how petroleum sulfonate collects fluorite with surface heterogeneity remains unknown. Therefore, in this study, ordinary sodium dodecyl sulfonate (C12S) was used as an alkyl sulfonate to collect fluorite with edge and vacancy in a computational manner, and the adsorption configuration of alkyl sulfonates on different crystal faces of fluorite and their interaction with the surface orbit of fluorite, as well as the interaction between alkyl sulfonates and vacancies on the surface of fluorite, was studied using DFT calculations.

## 2. Materials and Methods

### 2.1. Model and Parameters

The crystal and surface models of fluorite, the molecular models of the reagents, and the surface models of their interactions were all built using the Visualizer and Amorphous cells in Materials Studio. The first principle calculation was carried out in CASTEP package [22], including the structural optimization of the model and the calculation of charge density, differential charge, density of states, and other properties.

The dispersion force was corrected by TS [23]. The standard for self-consistent field convergence was  $1.0 \times 10^{-6}$  eV/atom, using OTFG [24] ultrasoft pseudopotential. All other simulation parameters remained in their default settings.

The surfaces were all cut out of fluorite crystal cells after structural optimization. After establishing a supercell, the surface area was about  $10 \times 10$  Å. A 55 Å vacuum layer was added above the surface, and a 3 Å vacuum layer was added below the bottom surface to avoid periodic imaging at the top of the model. The construction process is shown in Figure 1.

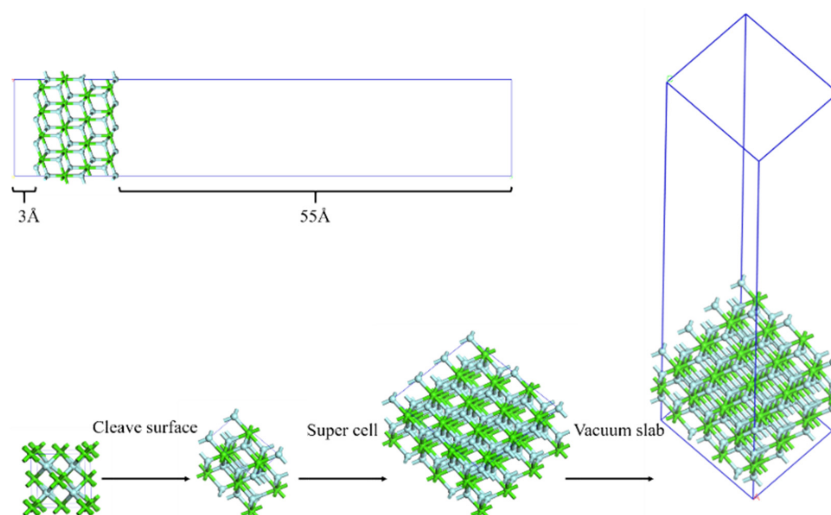


**Figure 1.** DFT calculations in the surface model construction process.

Firstly, adsorption models of fluorite (1 1 0), (1 1 1), and (3 1 1) surfaces with C12S were established. Among them, (1 1 0) and (3 1 1) surfaces were studied and analyzed as edges. Secondly, the surface model of fluorite (1 1 1) \_vacancy was established. The models are shown in Figures 2 and 3.

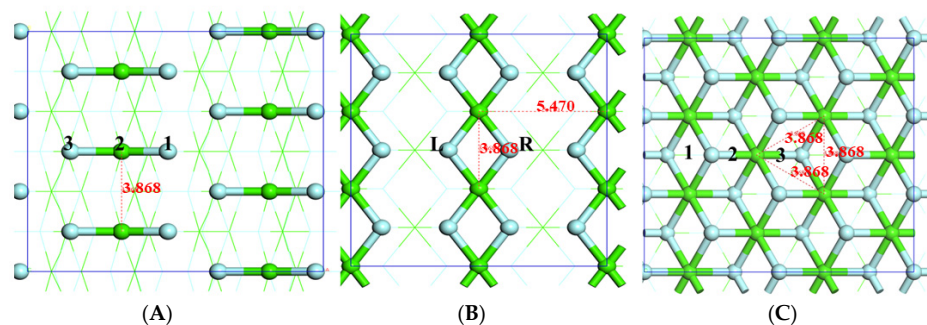


**Figure 2.** (A) Fluorite (3 1 1) surface structure: 1, upper fluorine atom; 2, middle calcium atom; 3, bottom fluorine atom. (B) Fluorite (1 1 0) surface structure: L, left fluoride atom; R, right fluoride atom. (C) Fluorite (1 1 1) surface structure: 1, upper fluorine atom; 2, middle calcium atom; 3, bottom fluorine atom.

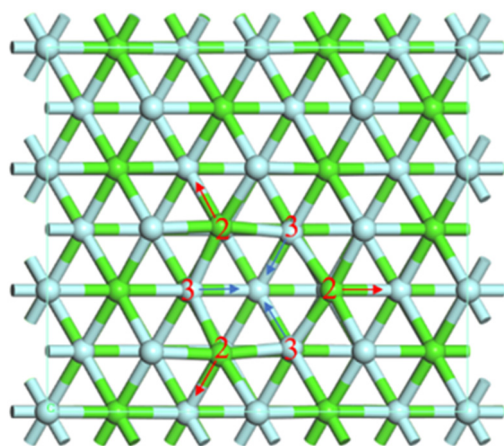


**Figure 3.** The (1 1 1) surface: 1, vacancy; 2, intermediate layer calcium atom; 3, lower layer fluorine atom.

After the truncation energy test of each exchange correlation function, GGA\_PBE [25], the convergence value of GGA\_PBE was the closest to the experimental value, and the error was only 0.12%, which is within the acceptable range, so GGA\_PBE was selected as the exchange correlation function. The truncation energy was 500 eV, and the k-point for all three surface settings was  $2 \times 2 \times 1$ . The BFGS [26] was used to optimize the structure in the process of simulation with the CASTEP package. The convergence conditions for structural optimization were as follows: energy  $1.0 \times 10^{-5}$  eV/atom, max. force 0.03 eV/Å, max. stress 0.05 GPa, max. displacement 0.001 Å. After structure optimization, the adsorption configuration and the changes in the structural parameters before and after adsorption were analyzed, and the adsorption energy, differential charge, and density of states were analyzed by single-point energy calculation.

## 2.2. Adsorption Energy Calculation

The adsorption energy of the collector on the fluorite surface was calculated using the following formula, in which the energy is calculated as single-point energy in the CASTEP package [22,27].

$$E_{\text{adsorption}} = E_{\text{after}} - (E_{\text{surface}} + E_{\text{reagent}}) \quad (1)$$

$E_{\text{adsorption}}$ : Adsorption energy of reagent on mineral surface.

$E_{\text{after}}$ : Total energy of reagent and mineral surface during stable adsorption.

$E_{\text{surface}}$ : Energy of mineral surface before adsorption.

$E_{\text{reagent}}$ : Energy of reagent before adsorption.

## 3. Results

### 3.1. Structural Analysis

The stable adsorption configurations of C12S on common exposed surfaces of fluorite after geometry optimization are shown in Figure 4. The stable adsorption configurations of C12S on (1 1 0) and (3 1 1) planes were in a bridged mode, while the adsorption configuration on (1 1 1) surface was in a monodentate mode [28].

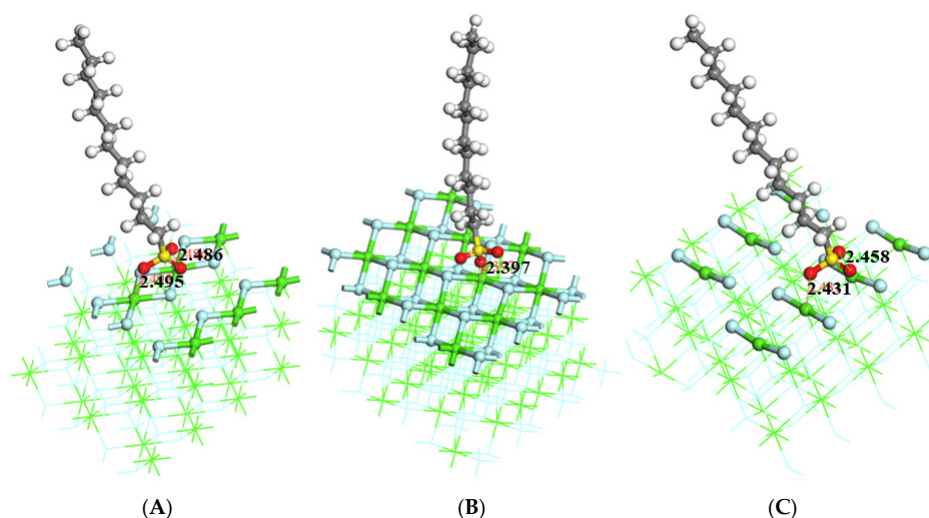


**Figure 4.** (A) Stable adsorption configuration of C12S on the fluorite (1 1 0) surface. (B) Stable adsorption configuration of C12S on the fluorite (1 1 1) surface. (C) Stable adsorption configuration of C12S on the fluorite (3 1 1) surface.

The detailed structures of the three fluorite surfaces are shown in Figure 5. When the collector structure was determined, the adsorption configurations were mainly determined by the atomic arrangement structure at the top layer of a certain mineral exposed surface. Compared with the (1 1 0) and (3 1 1) surfaces, calcium ions on the (1 1 1) surface were closely surrounded by fluorine ions, which were distributed as an equilateral triangle above and below it. The polar side of the dissociated C12S was a negatively charged sulfo group, which had the same structure as the fluorine ions on the (1 1 1) surface. Calcium ions will attract, while fluorine ions will repel, the C12S. As a balance of the repulsion and attractive forces, the adsorption configuration was monodentate. Although tridentate adsorption could also exist at the (1 1 1) surface, it had a strict requirement for the initial configuration. For the (1 1 0) and (3 1 1) surfaces, the distance of adjacent calcium was the same as the (1 1 1) surface, but the exposed degrees of these surfaces were different. There was no evidence of fluorine ions hindering the increase at another adsorption site, but the structure did not meet the requirement of tridentate adsorption, even at the two edge types of the (1 1 1) surface. As for the (1 1 1)<sub>vacancy</sub> surface, the dissolution of top-layer fluorine ions also resulted in the structuring of calcium ions in an equilateral triangle distribution that perfectly matched the sulfo group on C12S; so, the equalized adsorption configuration was tridentate adsorption.

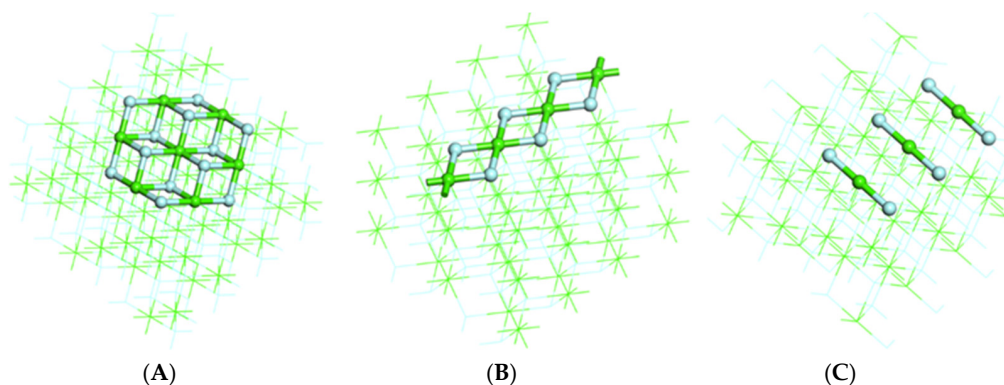


**Figure 5.** (A) Detailed structure of a fluorine ion surrounding calcium ions on the fluorite (1 1 0) surface. (B) Detailed structure of a fluorine ion surrounding calcium ions on the fluorite (1 1 1) surface. (C) Detailed structure of a fluorine ion surrounding calcium ions on the fluorite (3 1 1) surface.

The bond length and average bond length results of the C12S adsorption configuration on each surface are listed in Table 1. The results do not conclude a specific rule between the average bond length and bonding number. Although the adsorption configurations of C12S on (1 1 0) and (3 1 1) surfaces are the same, the average bond length of C12S on the (1 1 0) surface was greater than that of C12S on the (3 1 1) surface. The reason for this may be that the repulsion forces from the negatively charged fluorine ions of the (1 1 0) and (3 1 1) surfaces were different. The bonded C12S on the (1 1 0) surface received a stronger repulsion force, since the remaining oxygen atoms of the sulfo group repel fluorine ions, while the C12S on the (3 1 1) surface did not. In addition to the adsorption, the average bond length was also directly determined by the atomic arrangement of the exposed surface.

**Table 1.** Surface energy of different surfaces and average bond lengths of C12S on three surfaces.

Surface	Bond Length (Å)		Average Bond Length (Å)	Surface Energy (eV)
(1 1 1)	2.397		2.397	−84,052.59
(1 1 0)	2.495	2.486	2.492	−112,076.89
(3 1 1)	2.431	2.458	2.445	−84,041.33
(1 1 1) _vacancy	-	-	2.331	−111,437.02

According to the Db (surface broken bonds density) theory proposed by Gao et al. [22], the activity of calcium ions on the (1 1 1) surface was smaller than that on the (1 1 0) and (3 1 1) surface.

Figure 6 shows the stable adsorption configuration of C12S on the fluorite (1 1 1) surface vacancy after DFT calculations. The stable adsorption configuration of C12S on the fluorite (1 1 1) surface was in monodentate mode. The main obstacle to the bonding of residual oxygen atoms of the sulfo groups was the repulsion of fluorine ions on the fluorite (1 1 1) surface. Compared with the fluorite (1 1 1) surface, the vacancy formed by fluorine ion dissolution was more concentrated in the positive charge and more attractive to the collector. Moreover, the positively charged calcium ions in the vacancy exhibited an equilateral triangle distribution, and the geometric matching degree between the C12S and sulfo group was higher. Therefore, the stable adsorption configuration of C12S at the vacancy of the fluorite (1 1 1) surface was tridentate adsorption.

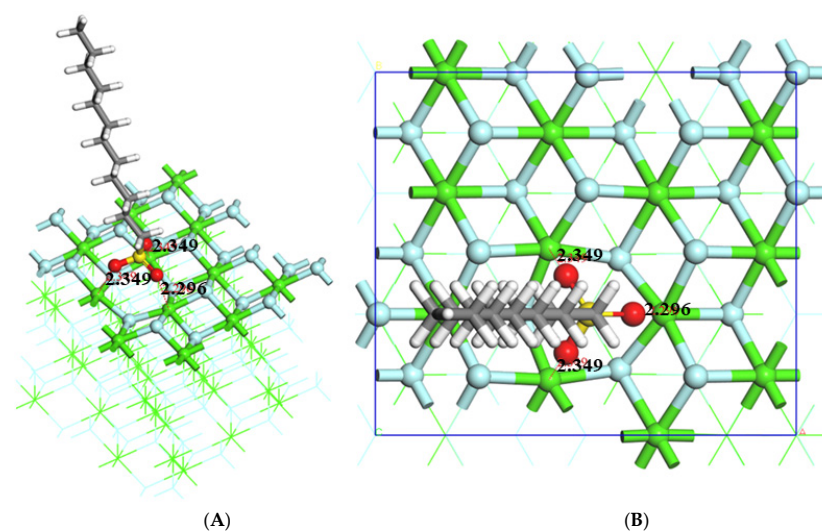


**Figure 6.** (A) Adsorption configuration of C12S on the fluorite (1 1 1) surface vacancy. (B) Bottom enlarged view.

### 3.2. Comparison of Adsorption Energy and Bond Length

Table 2 shows the adsorption energy calculation of C12S on different surfaces. Table 3 shows the relationship between the adsorption energy of C12S on different surfaces, the average bond length, and the number of bonding atoms.

**Table 2.** The adsorption energy calculation of C12S on different surfaces.

Surface	C12S (eV)	Surface (eV)	C12S + Surface (eV)	Adsorption Energy (eV)
(1 1 1)	−3914.47	−84,035.9	−87,951.26	−0.89
(1 1 0)	−3913.21	−112,054.92	−115,969.59	−1.46
(3 1 1)	−3914.55	−84,024.3	−87,940.39	−1.54
(1 1 1) _vacancy	−3914.54	−111,388.99	−115,310.28	−6.75

**Table 3.** The relationship between the adsorption energy of C12S on different surfaces, the average bond length, and the number of bonding atoms.

Surface	Adsorption Energy (eV)	Average Bond Length (Å)	Bonding Atoms
(1 1 1)	−0.89	2.492	2
(1 1 0)	−1.46	2.397	1
(3 1 1)	−1.54	2.445	2
(1 1 1) _vacancy	−6.75	2.331	3

First, from the perspective of bond length, the (1 1 0) surface had the longest bond length and the lowest adsorption energy, while the (1 1 1) surface had the shortest vacancy bond length and the highest adsorption energy. However, the bond length was not proportional to the adsorption energy, because the (3 1 1) surface was longer than the (1 1 1) surface, but the adsorption energy was higher.

Second, combined with the analysis of the number of coordination atoms, the adsorption energy of the (1 1 0) surface with the same two bonding atoms to C12S was lower than that of the (1 1 1) surface with only one bonding atom to C12S, while the adsorption energy of the (3 1 1) surface with the same two bonding atoms to C12S was higher than that of the (1 1 1) surface. Third, combined with the density of states analysis, the calcium atom on the surface exhibited electrostatic adsorption to the reagent, while the fluorine atom on the surface exhibited electrostatic repulsion, and the two acted together to form the adsorption. Because there were two fluorine atoms aligned with the oxygen atom on C12S at the (1 1 0) surface, its strong repulsion made its adsorption energy with C12S lowest. Because the dislocation of fluorine atoms and oxygen atoms, the repulsion of the (3 1 1) surface was weak, and its adsorption energy was higher than that of the (1 1 0) surface. The (1 1 1) surface with fluorine atom vacancy was due to the absence of fluorine atoms and the tridentate bonding, which only strongly adsorbs C12S, so its surface adsorption energy was the highest.

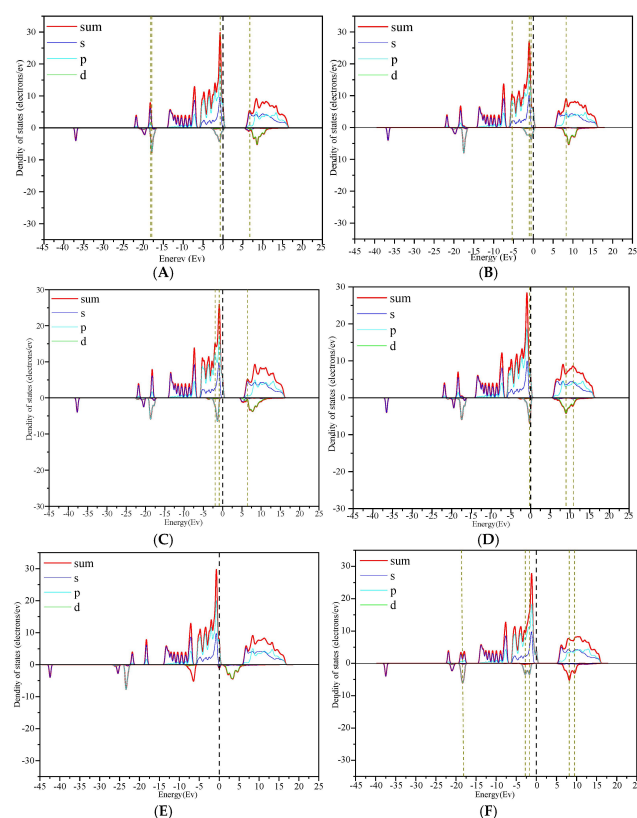
Thus, the average bond length of each surface did not correspond to its adsorption energy one by one. Also, the adsorption energy of the bridged mode was not necessarily lower than that of the monodentate mode, and the adsorption energy of the tridentate mode was the highest.

### 3.3. Density of State Analysis

The interaction between collector and mineral surface includes electrostatic force, chemical adsorption, and dispersive force. Anionic collectors, such as fatty acids and alkyl sulfonates, mainly interact with the calcium active sites on the mineral surface when collecting calcium-bearing minerals, and both undergo chemical adsorption [29,30]. The process of chemical adsorption is often accompanied by the electronic relationship between

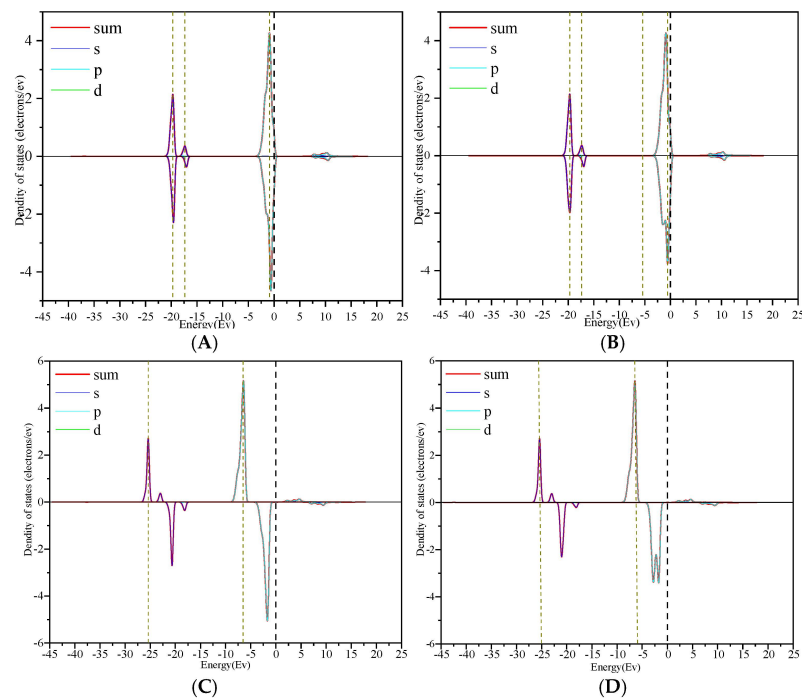
reagent molecules and minerals. Therefore, the analysis of the interaction between alkyl sulfonate and atomic orbits on the fluorite surface is helpful in revealing the chemical interaction form between the alkyl sulfonate collector and fluorite surface. Based on the analysis of fluorite crystals and atomic orbits on the fluorite surface, the changes in the density of states before and after the interaction between different mineral surfaces and sodium dodecyl sulfonate were analyzed, and the differences in chemical adsorption activities between common exposed surfaces of fluorite and alkyl sulfonate were compared.

Figure 7 displays the comparison of the density of states of the two kinds of edges and vacancies before and after the adsorption of C12S. Figures 8–11 show the comparison of the density of states of C12S and its bonded atoms on the two kinds of edges and vacancies before and after the adsorption. In order to explore the interaction between C12S molecules and fluorite surface atoms, the density of states of C12S and its bonded atoms on three surfaces were compared and analyzed before and after adsorption. Since the fluorite (3 1 1) surface was composed of upper and lower layers of fluorine ions and calcium ions in the middle layer, the fluorine ions in the upper layer were marked as 1F, the calcium ions in the middle layer were marked as 2Ca, and the fluorine ions in the third layer were marked as 3F. As the calcium ions in the surface layer of fluorite (1 1 0) were in the same plane as fluorine ions, the fluorine ions on the right side of calcium ions were marked as RF, the fluorine ions on the left was labeled LF. In addition, because the sulfonate and (3 1 1) and (1 1 0) surfaces exhibited double coordination adsorption, 1Ca represented the first calcium atom bonded, 2Ca represented the second calcium atom, 11F represented the upper fluorine ion of 1Ca, 13F represented the lower fluorine ion of 1Ca, 21F represented the upper fluorine ion of 2Ca, and 23F represented the lower fluorine ion of 2Ca.



**Figure 7.** (A) Comparison of density of states of fluorite (1 1 0) before interaction with C12S. (B) Comparison of density of states of fluorite (1 1 0) after interaction with C12S. (C) Comparison of density of states of fluorite (3 1 1) before interaction with C12S. (D) Comparison of density of states of fluorite (3 1 1) after interaction with C12S. (E) Comparison of density of states of fluorite (1 1 1) \_vacancy before interaction with C12S. (F) Comparison of density of states of fluorite (1 1 1) \_vacancy after interaction with C12S.





**Figure 8.** (A) Comparison of density of states between fluorite (1 1 0) \_LF and C12S before and after interaction. (B) Comparison of density of states between fluorite (1 1 0) \_RF and C12S after interaction. (C) Comparison of density of states between fluorite (1 1 1) \_vacancy\_1F and C12S before interaction. (D) Comparison of density of states between fluorite (1 1 1) \_vacancy\_3F and C12S after interaction.

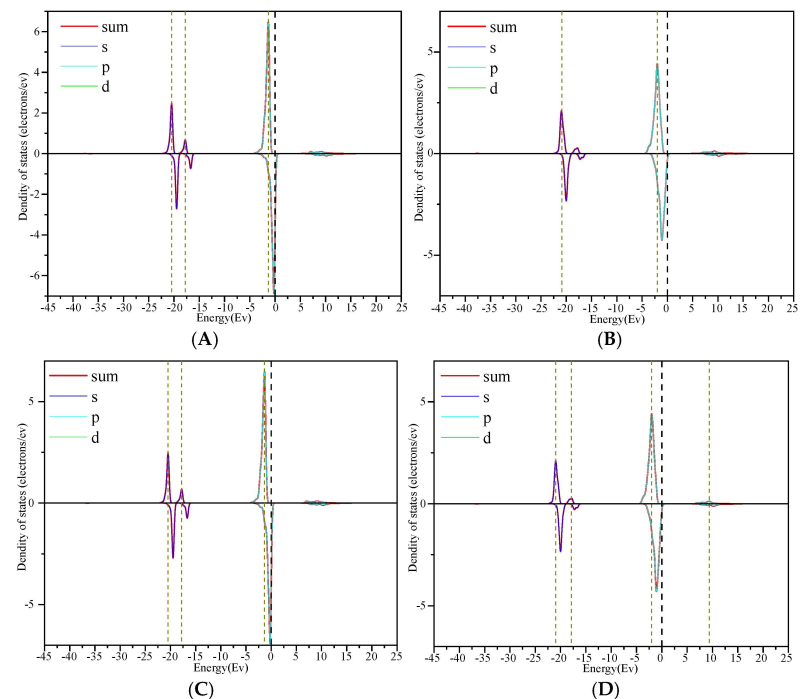


**Figure 9.** (A) Comparison of density of states between fluorite (3 1 1) \_11F and C12S before and after interaction. (B) Comparison of density of states between fluorite (3 1 1) \_13F and C12S before and after interaction. (C) Comparison of density of states between fluorite (3 1 1) \_21F and C12S before and after interaction. (D) Comparison of density of states between fluorite (3 1 1) \_23F and C12S before and after interaction.

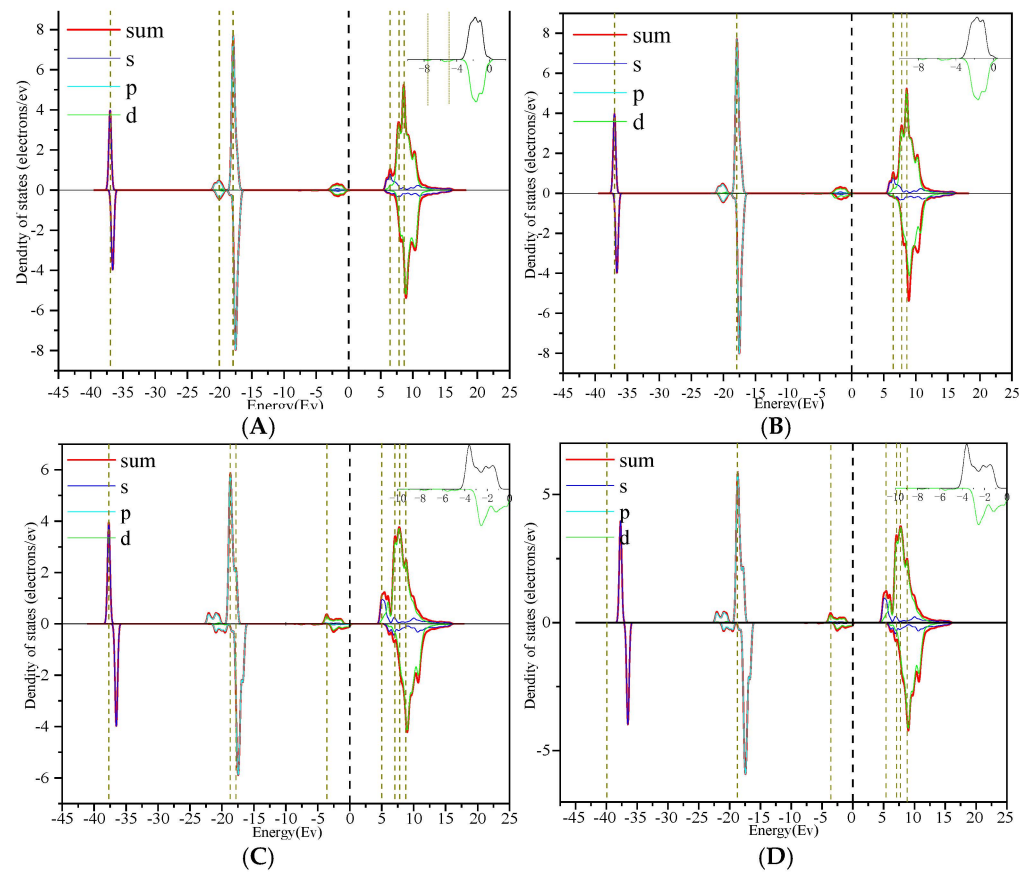


**Figure 10.** (A,B) Comparison of density of states between calcium atoms on the surface of fluorite (1 1 0) and C12S before and after interaction. (C,D) Comparison of density of states between calcium atoms on the surface of fluorite (3 1 1) and C12S before and after interaction.

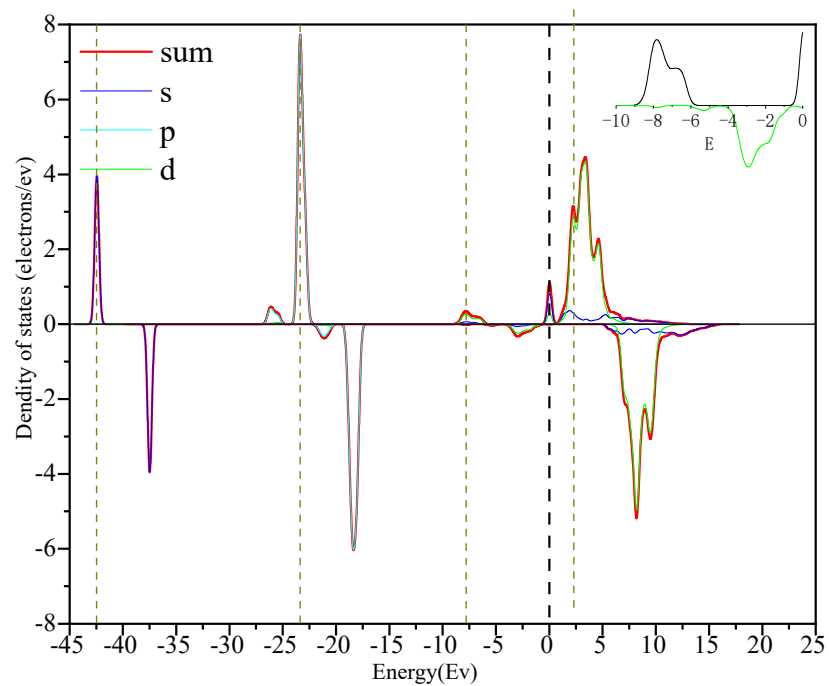


**Figure 11.** Comparison of density of states between calcium atoms on the surface of (1 1 1)<sub>vacancy</sub> and C12S before and after interaction.

For fluorine ions, the 2p orbit of the bottom fluorine ion at the vacancy was split, while the fluorine atom in the upper layer outside the vacancy showed no obvious change. The change in the fluorine ion 2p orbit on the surface of the edge was relatively complex, and was greatly affected by the surface structure. The interaction between the fluorine ion 2p orbit at  $-0.89$  eV and the collector molecular orbit below  $-0.89$  eV ( $-4.64$  eV and  $-1.92$  eV) pushed it to the high energy level, while the interaction with the collector molecular orbit above  $-0.89$  eV caused it to move to the low energy level. Both interactions broadened the fluorine ion 2p orbit below the Fermi level. Some electrons were lost after crossing the Fermi level, which hindered the adsorption. The orbit change of the fluorine ions on the (1 1 0) surface was the most significant, and the orbit change degree at the high energy level was greater than that at the low energy level, especially near the Fermi level. Among the three kinds of surfaces, only the fluorine ions after the action of the (1 1 0) surface had the phenomenon of peak to low-energy splitting, which was due to the repulsion between the fluorine ions on the right side of the (1 1 0) surface and the oxygen atoms not bonded by the sulfo group. In addition, the orbit change degree of the 1F on the (3 1 1) surface was greater than that of the 3F. This is consistent with the adsorption configurations of C12S on (1 1 0) and (3 1 1), that is, the fluorine ion orbit on the side of the unbound oxygen atom on the sulfo group changed significantly.

Compared to fluoride ions, the interaction between the 3d orbit of calcium ions above the Fermi level and the orbit of collectors at the Fermi level was stronger. The peak shape of the 3d orbit had better resonance with collectors, and the 3d orbit below the Fermi level widened to the low energy level and interacted with the orbits of collectors at  $-4.75$  eV and  $-7.11$  eV. The 2p orbit of calcium ions on the surface of the edge interacted with the molecular orbit of C12S at  $-18.27$  eV, which led to the increase in 2p orbit energy of calcium ions and the slight decrease in orbit energy of C12S molecules. The 4s orbit moved to the high energy level, indicating that it interacted with the orbit of the collector. The 3d orbit of calcium ions was located above the Fermi level, moved to the high energy level after interacting with the molecular orbit of the collector, and produced a good match with the orbit of the collector above the Fermi level. The 3d orbit located below the Fermi level was broadened to the lower energy level, and resonated with the collector molecular orbits located at  $-7.11$  eV and  $-4.78$  eV. The phenomena show that the 4s and 3d orbits of calcium ions interacted with the molecular orbits near collectors  $-7.11$  eV and  $-4.78$  eV, which were above the Fermi level. The 3d orbits of calcium ions extended to the low energy level, and was filled with electrons. The reduction in orbit energy and the filling of empty orbit could reduce the energy, which would be beneficial to the adsorption process. The deformation degree of the 3d orbits of calcium ions above the Fermi level was  $(3\ 1\ 1) > (1\ 1\ 1) > (1\ 1\ 0)$ , indicating that the interaction between the collector and calcium ions on the (3 1 1) surface was the largest.

### 3.4. Electron Difference

Figure 12 shows the electron difference of C12S adsorbed on the three surfaces of fluorite and surface vacancy, respectively. Among them, the lost electrons are displayed in blue and the obtained electrons are displayed in red.

For the (3 1 1) and (1 1 0) surfaces, the oxygen atom of the C12S molecule and the calcium ions on the surface gained electrons, while the sulfur atom of the collector and the fluorine ions on different surfaces lost electrons. This is consistent with the above results of the density of states analysis. Another visible trend is that the better the 3d orbits of calcium ions matched the orbits of collectors above the Fermi level, the larger the isosurface near the sulfur atom, indicating that more electrons were lost in the orbit. The number of electrons obtained by fluorine ions was also directly proportional to the degree of change in its density of states.

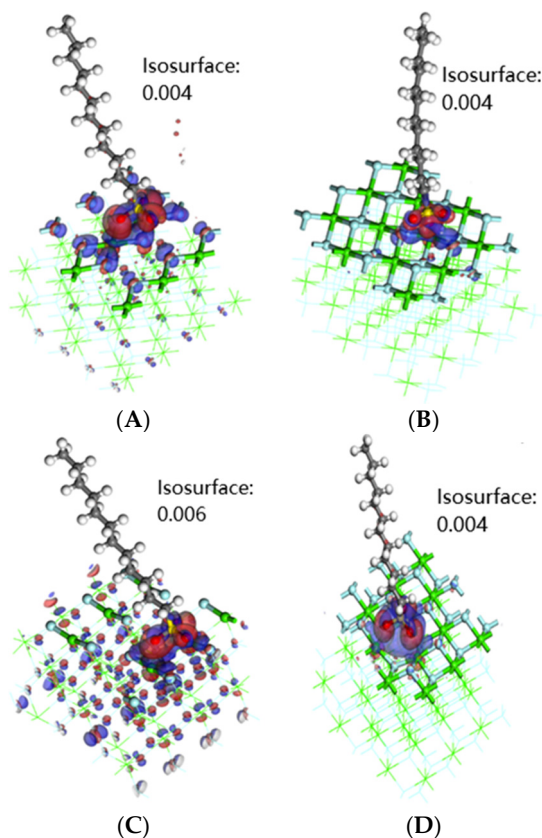


**Figure 12.** Electron difference of C12S adsorbed on fluorite surfaces: (A) electron difference of C12S adsorbed on the (1 1 0) surface; (B) electron difference of C12S adsorbed on the (1 1 1) surface; (C) electron difference of C12S adsorbed on the (3 1 1) surface; (D) electron difference of C12S adsorbed at the surface vacancy of the (1 1 1) surface.

For the (1 1 1) \_vacancy, the orbit near the collector's sulfur atom had a great tendency to lose electrons, while the tendency to gain electrons near the oxygen atom decreased; thus, the 3d orbit of the calcium ion matched the collector orbit best, and the 2p orbit of the fluorine ion did not extend above the Fermi level after reacting with the collector.

To sum up, both edges and vacancy were conducive to the adsorption of the reagent on the surface of fluorite. The collector had stronger adsorption on fluorite with a rough surface, and the existence of vacancy should improve the surface adsorption energy and enhance the adsorption of the agent on the surface. However, the rough mineral surface had a large specific surface area, which required high collector concentration to achieve saturated monolayer adsorption. Increasing vacancy is undoubtedly an effective method to improve the adsorption of sulfonate on fluorite surfaces.

#### 4. Conclusions

The DFT simulations of sodium dodecyl sulfonate adsorption on different surfaces and (1 1 1) \_vacancy of fluorite revealed the following:

- (1) The stable adsorption configuration of sodium dodecyl sulfonate on the (1 1 1) surface was in single coordination mode, while the stable adsorption configuration with edges was in bridge mode, and the stable action configuration with (1 1 1) \_vacancy was in tridentate mode. The interaction between sodium dodecyl sulfonate and several simulated surfaces and (1 1 1) \_vacancy was in the order of (1 1 1) \_vacancy > (3 1 1) > (1 1 1) > (1 1 0).
- (2) Through the analysis of the density of states and differential charges on the surfaces of edges and vacancy, the 2p orbit of fluorine had an obvious effect on the collector, and the electron was lost in the reaction process, which hinders the adsorption. The

3d orbits of calcium ions react with the anti-bonding orbits of collectors above the Fermi level, and then broaden to the low energy level, and resonate with their corresponding bonding orbits. Calcium gained some electrons in this process, which was beneficial to adsorption.

- (3) By comparing the adsorption energies and average bond lengths between different surfaces, the adsorption intensity of alkyl sulfonate on fluorite was found to be directly proportional to the action intensity of the collector on the 3d orbits of calcium ions on the surface and vacancy.
- (4) The existence of edges required a high collector concentration to achieve saturated monolayer adsorption. So, increasing the surface vacancy of fluorite is an effective method to improve the adsorption of sulfonate on fluorite surfaces. By using acid or alkali to etch the surface of fluorite, it may be possible to increase the vacancies on the fluorite surface, which would lead to improved flotation results.

**Author Contributions:** Y.H., Writing—original draft preparation, Writing—review and editing, Formal Analysis; Z.W., Conceptualization, Investigation; Z.R., Conceptualization, Methodology, Project Administration; R.Z., Writing—review and editing; H.G., Resources, Supervision; Z.C., Supervision, Writing—review and editing. All authors have read and agreed to the published version of the manuscript.

**Funding:** The authors acknowledge the financial support from the National Natural Science Foundation of China (Grant Nos. 51704219) and the Fundamental Research Funds for Central Universities (China, Grant No. WUT: 2022IV013h).

**Data Availability Statement:** This article does not provide new data, and all data can be used.

**Conflicts of Interest:** We declare that we do not have any commercial or associative interest that represent conflict of interest in connection with the work submitted.

## References

1. Zhu, L.; Liu, J.; Zhu, Y.; Gong, G.; Han, Y. Mechanism of HCA and CEPPA in flotation separation of cassiterite and fluorite. *Miner. Eng.* **2022**, *187*, 107773. [[CrossRef](#)]
2. Qian, Y.; Qiu, X.; Shen, T.; Huai, Y.; Chen, B.; Wang, Z. Effect of Calcium Ion on the Flotation of Fluorite and Calcite Using Sodium Oleate as Collector and Tannic Acid as Depressant. *Minerals* **2022**, *12*, 996. [[CrossRef](#)]
3. Wang, R.; Han, H.; Sun, W.; Nguyen, A.; Sun, W.; Wei, Z. Hydrophobic behavior of fluorite surface in strongly alkaline solution and its application in flotation. *Colloids Surf. A Physicochem. Eng. Asp.* **2021**, *609*, 125661. [[CrossRef](#)]
4. Chen, Z.; Ren, Z.; Gao, H.; Qian, Y.; Zheng, R. Effect of modified starch on separation of fluorite from barite using sodium oleate. *Physicochem. Probl. Miner. Process.* **2018**, *54*, 228–237.
5. Nikita, V.; Roman, Y.; Marina, F.; Igor, V.; Anatoly, N.; Vasily, D.; Dmitry, A. Crystal Chemistry, Isomorphism, and Thermal Conversions of Extra-Framework Components in Sodalite-Group Minerals. *Minerals* **2022**, *12*, 887.
6. Gao, Z.; Fan, R.; Ralston, J.; Sun, W.; Hu, Y. Surface broken bonds: An efficient way to assess the surface behavior of fluorite. *Miner. Eng.* **2019**, *130*, 15–23.
7. Zheng, R.; Ren, Z.; Gao, H.; Chen, Z.; Qian, Y.; Li, Y. Effects of crystal chemistry on sodium oleate adsorption on fluorite surface investigated by molecular dynamics simulation. *Miner. Eng.* **2018**, *124*, 77–85. [[CrossRef](#)]
8. Li, C.; Gao, Z. Tune surface physicochemical property of fluorite particles by regulating the exposure degree of crystal surfaces. *Miner. Eng.* **2018**, *128*, 123–132. [[CrossRef](#)]
9. Foucaud, Y.; Lebegue, S.; Filippov, L.; Filippova, I.V.; Badawi, M. Molecular Insight into Fatty Acid Adsorption on Bare and Hydrated (1 1 1) Fluorite Surface. *J. Phys. Chem. B* **2018**, *122*, 12403–12410. [[CrossRef](#)]
10. Motzer, C.; Reichling, M. Morphological classification and quantitative analysis of etch pits. *J. Appl. Phys.* **2010**, *108*, 113523. [[CrossRef](#)]
11. Pieper, H.; Barth, C.; Reichling, M. Characterization of atomic step structures on CaF<sub>2</sub> (1 1 1) by their electric potential. *Appl. Phys. Lett.* **2012**, *101*, 051601. [[CrossRef](#)]
12. Puchin, V.; Huisinga, M.; Reichling, M.; Puchina, A. Theoretical modelling of steps on the CaF<sub>2</sub> (1 1 1) surface. *J. Phys. Condens. Matter.* **2001**, *13*, 2081–2094. [[CrossRef](#)]
13. Kobayashi, N.; Itakura, S.; Asakawa, H.; Fukuma, H. Atomic-Scale Processes at the Fluorite–Water Interface Visualized by Frequency Modulation Atomic Force Microscopy. *J. Phys. Chem. C* **2013**, *117*, 24388–24396. [[CrossRef](#)]
14. de Leeuw, N.H.; Parker, S.C.; Rao, K.H. Modeling the Competitive Adsorption of Water and Methanoic Acid on Calcite and Fluorite Surfaces. *Langmuir* **1998**, *20*, 5900–5906. [[CrossRef](#)]

15. Dabringhaus, H.; Wandelt, K. Theoretical study of the adsorption of a  $\text{CaF}_2$  molecule at the (1 1 1) surface of  $\text{CaF}_2$  I. Equilibrium adsorption positions. *Surf. Sci.* **2003**, *526*, 257–272. [[CrossRef](#)]
16. Xu, B.; Wu, J.; Dong, Z.; Tao, J.; Qian, L.; Yang, Y. Flotation performance, structure–activity relationship and adsorption mechanism of a newly-synthesized collector for copper sulfide minerals in Gacun polymetallic ore. *Appl. Surf. Sci.* **2021**, *551*, 149420. [[CrossRef](#)]
17. Li, M.; Sun, B.; Ao, Z.; An, T.; Wang, G. Atomic-scale identification of influencing factors of sodium dendrite growth on different current collectors. *J. Mater. Chem. A* **2020**, *8*, 10199–10205. [[CrossRef](#)]
18. Weinberg, W.; Merrill, R. Crystal field surface orbit—Bond-energy bond-order (CFSO-BEBO) model for chemisorption: Application to hydrogen adsorption on a platinum (1 1 1) surface. *Surf. Sci.* **1972**, *33*, 493–515. [[CrossRef](#)]
19. Zhu, H.; Deng, H.; Chen, C. Flotation separation of andalusite from quartz using sodium petroleum sulfonate as collector. *Trans. Nonferrous Met. Soc. China* **2015**, *25*, 1279–1285. [[CrossRef](#)]
20. Jin, J.; Gao, H.; Ren, Z.; Chen, Z. The Flotation of Kyanite and Sillimanite with Sodium Oleate as the Collector. *Minerals* **2016**, *6*, 90. [[CrossRef](#)]
21. Ren, Z.; Shen, Y.; Gao, H.; Chen, H.; Liu, C.; Chen, Z. Comparison of Sodium Oleate and Sodium Petroleum Sulfonate for Low-Temperature Flotation of Fluorite and the Collecting Mechanisms. *Min. Met. Explor.* **2021**, *38*, 2527–2536. [[CrossRef](#)]
22. Clark, S.; Segall, M.; Pickard, C.; Hasnip, P.; Probert, M.; Refson, K.; Payne, M. First principles methods using CASTEP. *Z. Krist. Cryst. Mater.* **2005**, *220*, 567–570. [[CrossRef](#)]
23. Tkatchenko, A.; Scheffler, M. Accurate Molecular Van Der Waals Interactions from Ground-State Electron Density and Free-Atom Reference Data. *J. Phys. Rev. Lett.* **2009**, *102*, 073005. [[CrossRef](#)]
24. Li, S.; Liu, J.; Han, Y. Gene Properties of Barite (0 0 1) Surface Based on CASTEP Simulation. *Met. Mine* **2020**, *49*, 94–98.
25. Chen, Z.; Ren, Z.; Gao, H.; Lu, J.; Jin, J.; Min, F. The Effects of Calcium Ions on the Flotation of Sillimanite Using Dodecylammonium Chloride. *Minerals* **2017**, *7*, 28. [[CrossRef](#)]
26. Tankaria, H.; Sugimoto, S.; Yamashita, N. A regularized limited memory BFGS method for large-scale unconstrained optimization and its efficient implementations. *Comput. Optim. Appl.* **2022**, *82*, 61–68. [[CrossRef](#)]
27. Segall, M.; Lindan, P.; Probert, M.; Pickard, C.; Hasnip, P.; Clark, S.; Payne, M. First-principles simulation: Ideas, illustrations and the CASTEP code. *J. Phys. Condens. Matter.* **2002**, *14*, 2717. [[CrossRef](#)]
28. Gao, Z.; Li, C.; Sun, W.; Hu, Y. Anisotropic surface properties of calcite: A consideration of surface broken bonds. *Colloids Surf. A. Physicochem. Eng. Asp.* **2017**, *520*, 53–61. [[CrossRef](#)]
29. Marinalis, K.; Shergold, H. The mechanism of fatty acid adsorption in the presence of fluorite, calcite and barite. *Int. J. Miner. Process.* **1985**, *14*, 161–176. [[CrossRef](#)]
30. Chen, Z.; Ren, Z.; Gao, H.; Zheng, R.; Jin, Y.; Niu, G. Flotation studies of fluorite and barite with sodium petroleum sulfonate and sodium hexametaphosphate. *J. Mater. Res. Technol.* **2019**, *8*, 1267–1273. [[CrossRef](#)]

**Disclaimer/Publisher’s Note:** The statements, opinions and data contained in all publications are solely those of the individual author(s) and contributor(s) and not of MDPI and/or the editor(s). MDPI and/or the editor(s) disclaim responsibility for any injury to people or property resulting from any ideas, methods, instructions or products referred to in the content.